RESEARCH ARTICLE | AUGUST 23 2022

Fine and hyperfine interactions of PbF studied by laser-induced fluorescence spectroscopy

Chengcheng Zhu; Hailing Wang ; Ben Chen; Yini Chen; Tao Yang ; Jianping Yin ; Jinjun Liu

J. Chem. Phys. 157, 084307 (2022)
https://doi.org/10.1063/5.0099716
CHORUS

The Journal of Chemical Physics ARTICLE scitation.org/journal/jcp

Fine and hyperfine interactions of PbF studied by laser-induced fluorescence spectroscopy

Cite as: J. Chem. Phys. 157, 084307 (2022); doi: 10.1063/5.0099716
Submitted: 18 May 2022 • Accepted: 1 August 2022 •
Published Online: 23 August 2022

Chengcheng Zhu,[1] Hailing Wang,[1,a)] Ben Chen,[1] Yini Chen,[1] Tao Yang,[1] Jianping Yin,[1,a)] and Jinjun Liu[2,3]

AFFILIATIONS

[1] State Key Laboratory of Precision Spectroscopy, East China Normal University, 500 Dongchuan Road, Minhang District, 200241 Shanghai, People's Republic of China
[2] Department of Chemistry, University of Louisville, Louisville, Kentucky 40292, USA
[3] Department of Physics, University of Louisville, Louisville, Kentucky 40292, USA

[a)] **Authors to whom correspondence should be addressed:** hlwang@phy.ecnu.edu.cn and jpyin@phy.ecnu.edu.cn

ABSTRACT

The fine and hyperfine interactions in PbF have been studied using the laser-induced fluorescence (LIF) spectroscopy method. Cold PbF molecular beam was produced by laser-ablating a Pb rod under jet-cooled conditions, followed by the reaction with SF_6. The LIF excitation spectrum of the (0, 0) band in the $B^2\Sigma^+$–$X^2\Pi_{1/2}$ system of the ^{208}PbF, ^{207}PbF, and ^{206}PbF isotopologues has been recorded with rotational, fine structure, and hyperfine-structure resolution. Transitions in the LIF spectrum were assigned and combined with the previous $X^2\Pi_{3/2}$–$X^2\Pi_{1/2}$ emission spectrum in the near-infrared region [Ziebarth *et al.*, J. Mol. Spectrosc. **191**, 108–116 (1998)] and the $X^2\Pi_{1/2}$ state pure rotational spectrum of PbF [Mawhorter *et al.*, Phys. Rev. A **84**, 022508 (2011)] in a global fit to derive the rotational, spin–orbit, spin–rotation, and hyperfine interaction parameters of the ground ($X^2\Pi_{1/2}$) and the excited ($B^2\Sigma^+$) electronic states. Molecular constants determined in the present work are compared with previously reported values. Particularly, the significance of the hyperfine parameters, $A_\perp$ and $A_\parallel$, of ^{207}Pb is discussed.

I. INTRODUCTION

Since the electron's electric dipole moment (*e*EDM) was hypothesized, the prediction and measurement of *e*EDM have attracted much attention from the scientific community.[1–5] Experimental detection of the *e*EDM would prove the time-reversal (T) symmetry violation and, hence, may lead to a modification of the Standard Model (SM). PbF, a paramagnetic molecule, has been proposed as an excellent candidate for the detection of *e*EDM.[6] The *e*EDM is usually determined from the energy level shift in external fields. Therefore, the energy level structures of PbF, especially its fine and hyperfine structures, are of great interest to molecular spectroscopists and atomic, molecular, and optical (AMO) physicists. The effective spin–rotational Hamiltonian, H_{sr}, of PbF in an $\Omega = 1/2$ state in the presence of external fields can be written as[7]

$$H_{sr} = BJ^2 - \Delta \boldsymbol{S}' \cdot J + \boldsymbol{I} \cdot \hat{\boldsymbol{A}} \cdot \boldsymbol{S}' + \left(W^d d_e\right)\boldsymbol{S}' \cdot \boldsymbol{n} - D\mathcal{E} \cdot \boldsymbol{n} + \mu_B \mathcal{B} \cdot \hat{\boldsymbol{G}} \cdot \boldsymbol{S}'. \quad (1)$$

The first two terms of Eq. (1) give the J-dependent part of the rotational energy including the Λ-doubling (or Ω-doubling), where B is the rotational constant, $\boldsymbol{J}$ is the total angular momentum excluding the nuclear spin, Δ is the Λ-doubling constant, and $\boldsymbol{S}'$ is the effective spin of the electron.[8] The third term describes the hyperfine interaction, where $\boldsymbol{I}$ is the nuclear spin and $\hat{\boldsymbol{A}}$ is the hyperfine interaction tensor. The fourth term represents the interaction between the *e*EDM (d_e) and the effective internal electric field (W^d), where $\boldsymbol{n}$ is the unit vector directed along the internuclear axis from the positively charged atom to the negative one. The fifth term is for the Stark interaction, where D is the permanent dipole moment of

the molecule and $\mathcal{E}$ is the external electric field. The final term is for the Zeeman interaction, where μ_B is the Bohr magneton, $\mathcal{B}$ is the external magnetic field, and the tensor $\hat{G}$—which is diagonal in the molecular principal-axis system—determines the strength of the Zeeman interaction. Since this Hamiltonian determines the energy level structure of the PbF molecule in electromagnetic fields, which is of significance for detecting *e*EDM-sensitive transitions, the determination of molecular parameters in Eq. (1) with high precision is essential to improve future *e*EDM measurements using PbF.

Spectroscopic studies on PbF started in the 1930s when Rochester reported the first vibrational spectroscopic study on this molecule.[9–22] Later, Lumley and Barrow analyzed the rotational structure of the $B^2\Sigma^+$–$X_2{}^2\Pi_{3/2}$, $B^2\Sigma^+$–$X_1{}^2\Pi_{1/2}$, and $A^2\Sigma^+$–$X_1{}^2\Pi_{1/2}$ transitions of ^{208}PbF and gave the rotational parameters of the $v = 0$ and 1 levels of each electronic state.[19] The high-resolution spectrum of the $X_2{}^2\Pi_{3/2}$–$X_1{}^2\Pi_{1/2}$ transition was studied in 1998.[20] In 2010, fine structure constants of the *D*, *E*, and *F* states of ^{208}PbF, ^{207}PbF, and ^{206}PbF were determined in a mass-resolved resonance-enhanced multiphoton ionization (REMPI) spectroscopic measurement.[21] In 2011, the hyperfine structure of the X_1 state of ^{208}PbF, ^{207}PbF, and ^{206}PbF was determined from pure rotational spectra.[22] However, the high-resolution laser-induced fluorescence (LIF) spectrum of the $B^2\Sigma^+$–$X^2\Pi_{1/2}$ transition and the hyperfine parameters of the $B^2\Sigma^+$ state have not been reported yet.

In the present work, a supersonic expanded PbF molecular beam was produced, and the spectrum of the (0, 0) band of its $B^2\Sigma^+$–$X^2\Pi_{1/2}$ transition was recorded using the LIF technique. Rotationally resolved transitions of the ^{208}PbF, ^{207}PbF, and ^{206}PbF isotopologues were assigned, and their molecular parameters were determined and compared with previously reported results.

Although the future PbF-based *e*EDM measurement utilizes its *X* state, it is critical to investigate its excited electronic states too. First, the energy level structure of the *X* state is perturbed by low-lying excited electronic states. Although the *X* state is a relatively isolated state, its molecular constants determined in fitting experimentally obtained spectra, e.g., the Λ-doubling constants, still contain contributions due to interactions with other electronic states, including the *B* state. Experimentally determined molecular constants can also be used to benchmark relativistic configuration interaction calculations of the low-lying electronic state of PbF. The $B^2\Sigma^+$ state of PbF is of special interest in that it is the lowest Rydberg state arising from the $\sigma^2\sigma_R\pi^4$ configuration, where σ_R is the lowest Rydberg orbital.[23] Therefore, the *B* state plays an important role in the valence-Rydberg mixing, which shall be considered in both spectroscopic analysis[24] and *ab initio* calculations.[25] In the present work, the *B*-state rotational and spin–rotation constants of PbF have been determined with better precision in fitting the high-resolution LIF spectrum, while the hyperfine constants are reported for the first time, adding important, new pieces of information to the study of this promising candidate for the search of *e*EDM using diatomic radicals.

II. EXPERIMENTAL

The PbF molecular beam was produced by the reaction of laser-ablated Pb plasma with SF_6. The $B^2\Sigma^+$–$X^2\Pi_{1/2}$ transition was measured using the LIF technique with resolved fine and hyperfine structures. A brief description of the experimental setup is given as follows.

The second harmonic output of a Nd:YAG laser (Quantel-Brilliant, 532 nm, 10 Hz repetition rate, pulse energy ~1 mJ) was focused onto a high-purity Pb rod (Alfa Aesar, 99.999%) that underwent a continuous rotational and translational motion. The Pb rod was polished to remove the oxide coating before it was installed in the source chamber. The gas mixture of SF_6/Ar (volume ratio, 5:95) passed through a pulsed nozzle valve and expanded into the source chamber to form a free jet expansion. The SF_6 molecule reacted with the ablated Pb plasma to produce the PbF molecule, which was excited from the ground ($X^2\Pi_{1/2}$) state to the $B^2\Sigma^+$ state by the frequency-doubled output from a tunable continuous-wave (CW) ring dye laser (Sirah, Matisse DS) in the detection chamber. The excitation laser beam was slightly focused to ~1 mm onto the molecular beam. The fluorescence following the $B^2\Sigma^+$–$X^2\Pi_{1/2}$ excitation of PbF was collected by a lens telescope system onto a photomultiplier tube (PMT, Sofn Instrument Co., 71D101-CR131). The PMT signal was amplified by a preamplifier (Standford Research System, SR240A), integrated using a boxcar system (Standford Research System, SR200 series), and sent to a personal computer (PC). The LIF spectrum was recorded by a home-written LabVIEW program.

The frequency of the CW dye laser was measured by a wavemeter (HighFinesse, WS-U) and calibrated using the Doppler-free saturation absorption spectrum molecular iodine during the spectral scan.

III. RESULTS

The high-resolution LIF spectrum of the $B^2\Sigma^+$–$X^2\Pi_{1/2}$ transition of PbF has been recorded in the frequency region of 35 686 –35 720 cm^{-1}. Totally, 336 spectral lines were identified and assigned in the present work. The experimental and simulated excitation spectra are compared in Fig. 1. The abundances of the four

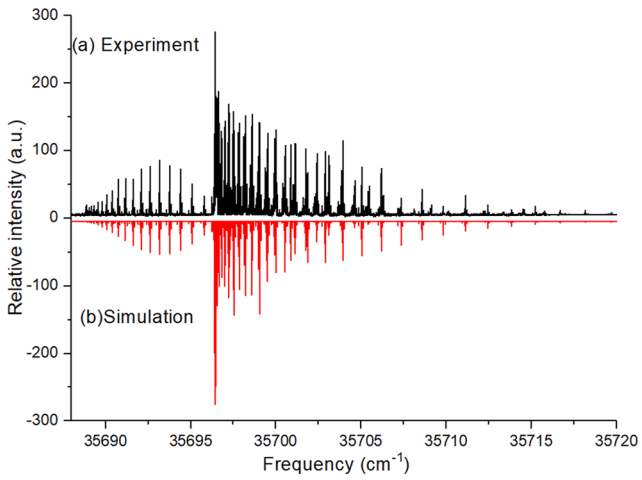

FIG. 1. Experimental (top) and simulated (bottom) spectra of the (0, 0) band of the $B^2\Sigma^+$–$X^2\Pi_{1/2}$ transition of PbF.

naturally occurring isotopes of Pb, ^{208}Pb(I = 0), ^{207}Pb(I = 1/2), ^{206}Pb(I = 0), and ^{204}Pb(I = 0) are 52.4%, 22.1%, 24.1%, and 1.4%, respectively. Transitions of ^{204}PbF are not identified in the present work due to its low abundance. The spectral linewidth (full width at half maximum, FWHM) of the recorded spectrum is ~0.007 cm^{-1}. The ^{19}F(I = 1/2) hyperfine splitting is not resolved in the recorded spectrum.

A portion of the P-branch of the experimental spectrum is shown in Fig. 2, in which transitions assigned to ^{208}PbF, ^{207}PbF, and ^{206}PbF are labeled. The notation used to label the transitions is defined similarly to the one given previously,[26,27] $^{\Delta N}\Delta J_{F'_iF''_i}(J)$, where $\boldsymbol{N} = \boldsymbol{J} - \boldsymbol{S}$ is the total angular momentum excluding both nuclear and electron spins. The first subscript, F_i', with i = 1, 2, corresponds to the upper ($J = N + 1/2$) and lower ($J = N - 1/2$) spin-rotation components of the $B^2\Sigma^+$state, respectively. The second subscript, F_i'', with i = 1, 2, corresponds to the lower ($X_1{}^2\Pi_{1/2}$) and upper ($X_2{}^2\Pi_{3/2}$) spin–orbit components of the $X^2\Pi$ state, respectively. When $F_i' = F_i''$, only one number is used.

For the ground $X^2\Pi_{1/2}$ state of ^{208}PbF and ^{206}PbF, Hund's case (a) angular momentum coupling scheme is used to describe its energy level structure.[20] The Hamiltonian includes the spin–orbit interaction (with the associated molecular constant, $\tilde{A}$) and its centrifugal distortion correction ($\tilde{A}_D$), the rotational Hamiltonian (B), the Λ-doubling (p, q),[26]

$$\boldsymbol{H}^{eff}(^2\Pi) = \tilde{A}L_zS_z + B\boldsymbol{N}^2 - \frac{1}{2}q\left(e^{-2i\phi}J_+^2 + e^{+2i\phi}J_-^2\right) - \frac{1}{2}(p+2q)\left(e^{-2i\phi}J_+S_+ + e^{+2i\phi}J_-S_-\right), \quad (2)$$

where J_+, J_-, S_+ and S_- are the shift operators and ϕ is the orbital azimuthal angle of the unpaired electron. Centrifugal distortion corrections to the three terms ($\tilde{A}_D$, $\tilde{A}_H$, D, q_D) have also been included in the spectral simulation and fitting, although they are not included in Eq. (2) for clarity. The readers are referred to Ref. 28 for details. The Λ-doubling parameter q is fixed to zero in the present work due to its negligible effect on the energy level structure.[22]

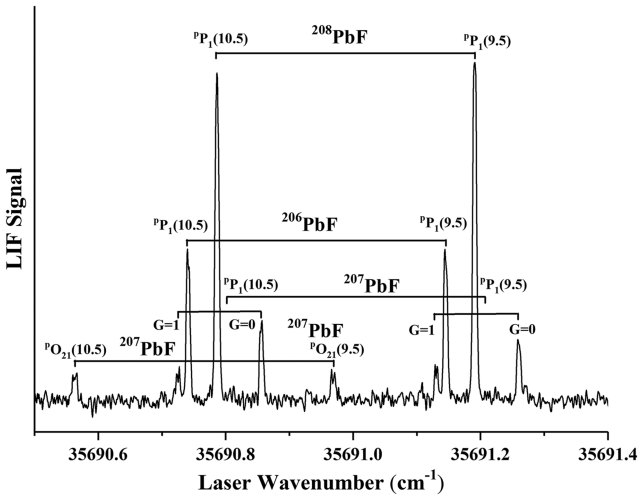

FIG. 2. A portion of P-branch of the $B^2\Sigma^+$–$X^2\Pi_{1/2}$ (0, 0) band of PbF. Assigned transitions of ^{208}PbF, ^{207}PbF, and ^{206}PbF are labeled.

For the $B^2\Sigma^+$ state of PbF, Hund case (b) is adopted. The Hamiltonian for the $B^2\Sigma^+$ state of ^{208}PbF and ^{206}PbF can be described as

$$H^{eff}(^2\Sigma) = T_{00} + B\boldsymbol{N}^2 + \gamma\boldsymbol{N}\cdot\boldsymbol{S}, \quad (3)$$

where the first term is the band origin, the second term is the rotation Hamiltonian (the centrifugal distortion correction has also been included in the spectral simulation and fitting), and the final term describes the spin–rotation interaction. There are six transition branches, ^{p}P$_1$, ^{q}P$_{21}$, ^{q}Q$_1$, ^{r}Q$_{21}$, ^{r}R$_1$, and ^{s}R$_{21}$ in the (0, 0) band of the $B^2\Sigma^+$–$X^2\Pi_{1/2}$ transition of ^{208}PbF and ^{206}PbF.

In the LIF spectrum of ^{207}PbF, the hyperfine splitting from the nuclear spin of ^{207}Pb(I = 1/2) is resolved. Hund's case ($a_{\beta J}$) coupling scheme is used in constructing the effective Hamiltonian of the $X^2\Pi$ state of ^{207}PbF,[26]

$$\boldsymbol{H}^{hf}(^2\Pi) = a(^{207}\mathrm{Pb})\boldsymbol{I}(^{207}\mathrm{Pb})_zL_z + \frac{1}{2}d(^{207}\mathrm{Pb}) \times \left[e^{-2i\phi}I(^{207}\mathrm{Pb})S_+ + e^{+2i\phi}I(^{207}\mathrm{Pb})S_-\right], \quad (4)$$

where $a(^{207}\mathrm{Pb})$ and $d(^{207}\mathrm{Pb})$ are the nuclear spin–electron orbit interaction constant and the constant for the dipole–dipole coupling between the nuclear spin and the electron spin, respectively.

For the $B^2\Sigma^+$ state of ^{207}PbF, Hund's case ($b_{\beta S}$) coupling scheme is used,[27]

$$\boldsymbol{H}^{hf}(^2\Sigma^+) = b_F(^{207}\mathrm{Pb})\boldsymbol{I}(^{207}\mathrm{Pb})\cdot\boldsymbol{S} + c(^{207}\mathrm{Pb})I(^{207}\mathrm{Pb})S_z, \quad (5)$$

where the Fermi contact constant $b_F(^{207}\mathrm{Pb})$ and the Frosch and Foley hyperfine constant $c(^{207}\mathrm{Pb})$ are adopted for the nuclear spin–electron spin interaction and the nuclear spin–electron spin dipole–dipole interaction, respectively.

In this Hund's case ($b_{\beta S}$) coupling scheme, the electron spin angular momentum $\boldsymbol{S}$(=1/2) is coupled to the nuclear spin of ^{207}Pb ($\boldsymbol{I}$ = 1/2) to give the total spin angular momentum $\boldsymbol{G}$, with the approximately good quantum numbers (G) having possible values of 1 and 0. $\boldsymbol{G}$ is coupled with $\boldsymbol{N}$ to give the total angular momentum $\boldsymbol{F}$. The aforementioned six branches of the $^2\Sigma^+(b)$–$X^2\Pi_{1/2}$ (a) labeling scheme regroup into eight branch features of the $^2\Sigma^+$ ($b_{\beta S}$)–$X^2\Pi_{1/2}$ ($a_{\beta J}$) scheme. Therefore, ^{207}PbF has eight branches,[29] ^{p}P$_1$, ^{q}P$_{21}$, ^{p}O$_{21}$, ^{q}Q$_1$, ^{r}Q$_{21}$, ^{r}R$_1$, ^{s}R$_{21}$, and ^{s}S$_1$ in the (0, 0) band of its $B^2\Sigma^+$–$X^2\Pi_{1/2}$ transition (see Fig. 2).

The spectrum of the (0, 0) band of the $B^2\Sigma^+$–$X^2\Pi_{1/2}$ system was simulated using the PGOPHER program.[29] Molecular constants of both the $X^2\Pi_{1/2}$ ground state and the $B^2\Sigma^+$ excited state of the three isotopologues of PbF determined in fitting the spectrum are listed in Tables I and II in comparison with previous values, wherever available.[19,20,22,30–33] Observed and calculated transition frequencies and residuals of the frequency fit are given in the supplementary material. The standard deviations of the fits for the ^{208}PbF, ^{207}PbF, and ^{206}PbF spectral lines are 0.0015, 0.0010, and

TABLE I. Molecular constants of the $X^2\Pi_{1/2}$ and $B^2\Sigma^+$ states of ^{206}PbF, ^{207}PbF, and ^{208}PbF (in the unit of cm^{-1}). The first value for each molecular constant listed is from a global fit to the $X^2\Pi_{3/2}$–$X^2\Pi_{1/2}$ spectrum of Ref. 20, the pure rotational spectrum of Ref. 22, and the $B^2\Sigma^+$–$X^2\Pi_{1/2}$ spectrum of the present work, while previously reported values are included in the other rows. The numbers in parentheses are error bars in the unit of the last digit.

State	Parameter	^{208}PbF	^{207}PbF	^{206}PbF
$X^2\Pi_{1/2}$	B''	0.230 646(3) 0.230 663 40(6)[a] 0.230 663(2)[b] 0.228 01(5)[c]	0.230 766(2) 0.230 756 67(3)[a] 0.230 751(5)[b]	0.230 850 7(6) 0.230 850 63(2)[a] 0.230 846(2)[b]
	$10^7 \times D''$	1.738(19) 1.826(2)[a] 1.823(5)[b] 1.81(5)[c]	1.900(41) 1.844(6)[a] 1.82(2)[b]	1.929(70) 1.817(6)[b]
	$\tilde{A}$	8 276.287 2(22) 8 276.283 5(6)[a] 8 276.283 59(9)[b]	8 276.291 02(51) 8 276.292 7(6)[a] 8 276.293 0(4)[b]	8 276.299 2(fixed) 8 276.299 2(9)[b]
	$10^3 \times \tilde{A}_D$	5.256 56(19) 5.256 8(1)[a] 5.256 8(2)[b]	5.265 36(51) 5.259 2(10)[a] 5.259 0(6)[b]	5.261 1(fixed) 5.261 1(2)[b]
	p	−0.137 919(8) −0.138 213 92(1)[a] −0.138 20(1)[b] −0.138 8(3)[c]	−0.138 269(2) −0.138 270 00(1)[a] −0.138 43(2)[b]	−0.138 326 8(1) −0.138 326 73(3)[a] −0.138 30(1)[b]
$B^2\Sigma^+$	B'	0.247 322 5(57) 0.247 36(5)[c]	0.247 449 5(76)	0.247 537 5(16)
	$10^7 \times D'$	1.617(15) 1.62(3)[c]	1.619(4)	1.475(23)
	γ	0.002 653(16) 0.002 6(1)[c]	0.002 732(13)	0.002 716(22)
	$b(^{207}\text{Pb})$		0.158 4(17)	
	$c(^{207}\text{Pb})$		0.006 0(4)	
T_{00}		31 558.949 7(3)	31 558.918 3(8)	31 558.902 2(2)

[a]Reference 22.
[b]Reference 20.
[c]Reference 19.

0.0011 cm^{-1}, respectively, which are significantly smaller than the FWHM of the LIF spectrum.

A global fit involving the field-free emission spectrum of the $X_2{}^2\Pi_{3/2}$–$X_1{}^2\Pi_{1/2}$ transition in the mid-infrared region,[20] the pure rotational microwave spectrum of the $X_1{}^2\Pi_{1/2}$ state,[22] and the LIF spectrum of the $B^2\Sigma^+$–$X^2\Pi_{1/2}$ recorded in this work has been carried out. Transition frequencies from different spectra were weighted according to their reported accuracies. Molecular constants of the ground ($X^2\Pi_{1/2}$) and the excited ($B^2\Sigma^+$) electronic states determined in the global fit are given in Table I. The spin–orbit constant ($\tilde{A}$) and its centrifugal distortion correction parameter ($\tilde{A}_D$) of the $X^2\Pi$ state of PbF determined in the present work are in good agreement with values previously reported in Refs. 20 and 22. The values for the $\tilde{A}_H$ and p_D of the $X^2\Pi_{1/2}$ state are fixed at the values reported in Ref. 22. For the $B^2\Sigma^+$ state, the spin–rotation constant (γ) has been reported in Ref. 19, albeit only for ^{208}PbF. Our results for the molecular constants of the $B^2\Sigma^+$ state of ^{208}PbF agree with Ref. 19. The experimentally determined values of the Frosch and Foley hyperfine constants, $b(^{207}\text{Pb})$ and $c(^{207}\text{Pb})$, of the $B^2\Sigma^+$ state are 0.1584(17) and 0.0060(4) cm^{-1}, respectively. The fine and hyperfine structure constants of the $B^2\Sigma^+$ state of ^{207}PbF and ^{206}PbF are determined for the first time in the present work.

TABLE II. The hyperfine constants, $A_\perp$ and $A_\parallel$, of ^{207}Pb in the ground state, $X^2\Pi_{1/2}$, and the excited state, $B^2\Sigma^+$ of ^{207}PbF (in the unit of cm^{-1}). The numbers in the parentheses denote the error bars in the unit of the last digit.

		$A_\perp(^{207}\mathrm{Pb})$	$A_\parallel(^{207}\mathrm{Pb})$
$X^2\Pi_{1/2}$	Our results (expt.)	−0.242 3(7)	0.338 0(12)
	Reference 21 (expt.)	−0.242 302 25(1)	0.338 456 59(3)
	Reference 20 (expt.)	0.242(1)	⋯
	Reference 30 (theo.)[a]	−0.239 3	0.331 6
	Reference 31 (theo.)[b]	−0.228 8	0.324 4
	Reference 32 (theo.)[c]	−0.262(13)	0.304(14)
	Reference 33 (theo.)[d]	−0.299 9	0.366 6
$B^2\Sigma^+$	Our results (expt.)	0.164 4(21)	0.158 4(17)

[a]The relativistic coupled-clusters method combined with the generalized relativistic effective core potential approach and nonvariational one-center restoration technique.
[b]The *ab initio* relativistic correlation method.
[c]The self-consistent field method.
[d]The *ab initio* effective core potential calculation method.

IV. DISCUSSION

Based on our experimental results, the energy level diagrams of $B^2\Sigma^+$ and $X^2\Pi_{1/2}$ states of PbF isotopologues can be derived. The energy level associated with the LIF transitions assigned in Fig. 2 are illustrated in Fig. 3 (for ^{208}PbF and ^{206}PbF) and Fig. 4 (for ^{207}PbF). The energy level diagrams for the $X^2\Pi_{1/2}$ state of the ^{208}PbF and ^{207}PbF show that these two isotopologues have small

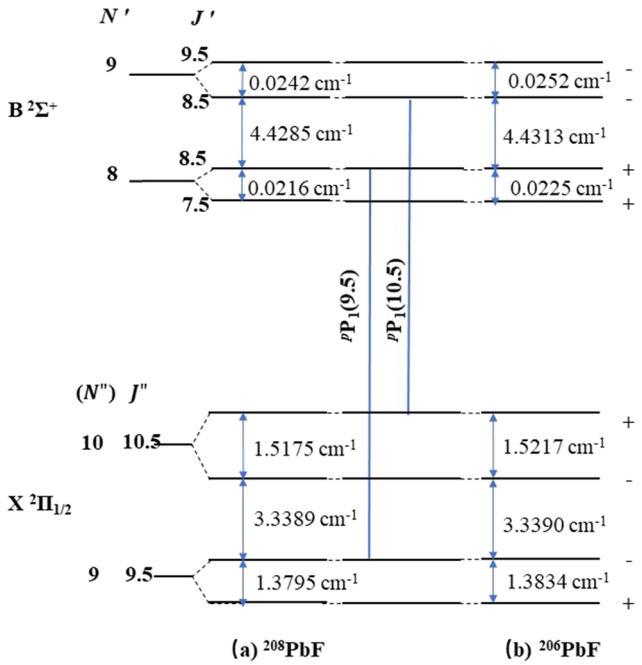

FIG. 3. Energy level structure and transition diagram of ^{208}PbF and ^{206}PbF associated with the transitions in Fig. 2.

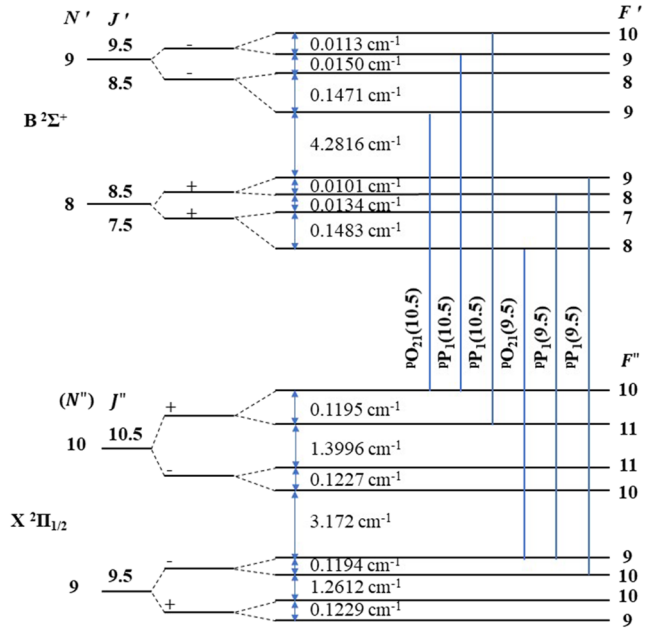

FIG. 4. Energy level structure and transition diagram of ^{207}PbF associated with the transitions in Fig. 2.

Λ-doubling splittings. In the *e*EDM measurement, a sufficient external field is required to mix the ground state Λ-doubling levels. Therefore, the nearly degenerated lowest-lying Λ-doubling levels of the ^{208}PbF and ^{207}PbF could have advantages for the PbF-based *e*EDM measurement.

The hyperfine interaction tensor $\hat{A}$ [see Eq. (1)] is diagonal in the molecular frame and can be parameterized as $A_\perp$ and $A_\parallel$ by combining the Frosch and Foley hyperfine constants.[6] For the $X^2\Pi_{1/2}$ state of ^{207}PbF, $A_\perp(^{207}\mathrm{Pb}) = -d$ and $A_\parallel(^{207}\mathrm{Pb}) = 2a - b - c$.[22] We derived $A_\perp(^{207}\mathrm{Pb}) = -0.2423(7)$ cm^{-1} from our experimental results (see Table I). The Frosch and Foley hyperfine constants, b and c, in the $X^2\Pi_{1/2}$ state are negligible and, hence, were set to zero in our fits. As a result, $A_\parallel(^{207}\mathrm{Pb})$ is given as 0.3380(12) cm^{-1}. The $A_\perp(^{207}\mathrm{Pb})$ and $A_\parallel(^{207}\mathrm{Pb})$ of the $X^2\Pi_{1/2}$ state of ^{207}PbF are listed and compared with previously determined values in Table II. Our $A_\perp$ and $A_\parallel$ values are in good agreement with the experimental results derived for the $X^2\Pi_{1/2}$ state in Ref. 22. The discrepancy in the sign of $A_\perp$ in Ref. 20 is caused by different sign conventions in the expression of the energy levels.[22] The theoretically predicted values are slightly larger than ours and previously reported experimental ones. Moreover, we have derived the values of the $A_\perp(^{207}\mathrm{Pb}) = 0.1584(17)$ and $A_\parallel(^{207}\mathrm{Pb}) = 0.1644(21)$ cm^{-1} for the $B^2\Sigma^+$ state of ^{207}PbF from our experimental results (see Table II). Currently, only McRaven *et al.*[17] and Baklanov *et al.*[31] have reported the experimental and theoretical results of the $A_\perp(^{207}\mathrm{Pb})$ and $A_\parallel(^{207}\mathrm{Pb})$ of the $A^2\Sigma^+$ state. There are no reported values of the $A_\perp(^{207}\mathrm{Pb})$ and $A_\parallel(^{207}\mathrm{Pb})$ of the $B^2\Sigma^+$ state in the literature.

In the fourth term of Eq. (1), $\left(W^d d_e\right)\boldsymbol{S}'\cdot\boldsymbol{n}$, the nonzero value of d_e can be measured experimentally. However, the effective internal electric field (W^d) can only be predicted by high-level electronic

structure calculations. A comparison of the experimentally determined values of the $A_\perp(^{207}\mathrm{Pb})$ and $A_\parallel(^{207}\mathrm{Pb})$ reported in the present work can help test the reliability of computational methodologies for predicting W^d. The same *ab initio* relativistic correlation methods for calculating W^d can also predict the Fermi contact interaction constant $b_F = b + c/3$.[21] In this work, the experimentally determined $b_F(^{207}\mathrm{Pb})$ is 0.1604(18) cm^{-1}, which can also be used to test theoretical methods for predicting W^d.

V. CONCLUSIONS

In summary, we recorded the high-resolution LIF spectrum of the (0, 0) band of the $B^2\Sigma^+$–$X^2\Pi_{1/2}$ transition of PbF under jet-cooled conditions and studied the fine and hyperfine interactions in its $B^2\Sigma^+$ and $X^2\Pi_{1/2}$ states. The spectral lines of ^{208}PbF, ^{207}PbF, and ^{206}PbF were assigned and analyzed to derive the fine and hyperfine molecular parameters of the $v = 0$ levels of the $B^2\Sigma^+$ and $X^2\Pi_{1/2}$ states of all three isotopologues. The hyperfine parameters, $A_\perp$ and $A_\parallel$, of the $X^2\Pi_{1/2}$ and $B^2\Sigma^+$ states of ^{207}PbF were given and discussed. The Fermi contact interaction constant (b_F) of the $B^2\Sigma^+$ state of ^{207}PbF was determined for the first time in the present work. These parameters are essential in determining energy shifts in *e*EDM measurements and can be used to test theoretical methods in predicting the internal electric field of PbF.

SUPPLEMENTARY MATERIAL

See the supplementary material for the rotational assignment of experimentally observed spectral lines in the (0, 0) band of the $B^2\Sigma^+$–$X^2\Pi_{1/2}$ transition of ^{208}PbF, ^{207}PbF, and ^{206}PbF (in units of cm^{-1}).

ACKNOWLEDGMENTS

This research was supported by grants received from the National Natural Science Foundation of China (Grant Nos. 11674096, 11834003, and 11874151). J.L. acknowledges financial support received from the NSF under Grant No. CHE-1955310.

AUTHOR DECLARATIONS

Conflict of Interest

The authors have no conflicts to disclose.

Author Contributions

Chengcheng Zhu: Data curation (equal); Investigation (equal); Writing – original draft (equal). **Hailing Wang**: Formal analysis (lead); Funding acquisition (lead); Supervision (equal); Writing – review & editing (equal). **Ben Chen**: Data curation (equal); Software (equal). **Yini Chen**: Investigation (equal); Software (equal). **Tao Yang**: Funding acquisition (supporting). **Jianping Yin**: Funding acquisition (supporting); Supervision (equal). **Jinjun Liu**: Funding acquisition (supporting); Formal analysis (supporting); Writing – review & editing (equal).

DATA AVAILABILITY

The data that support the findings of this study are available from the corresponding authors upon reasonable request.

REFERENCES

[1] S. K. Lamoreaux, J. P. Jacobs, B. R. Heckel, F. J. Raab, and N. Fortson, "New constraints on time-reversal asymmetry from a search for a permanent electric dipole moment of ^{199}Hg," Phys. Rev. Lett. **59**, 2275 (1987).
[2] J. J. Hudson, D. M. Kara, I. J. Smallman, B. E. Sauer, M. R. Tarbutt, and E. A. Hinds, "Improved measurement of the shape of the electron," Nature **473**, 493–496 (2011).
[3] W. B. Cairncross, D. N. Gresh, M. Grau, K. C. Cossel, T. S. Roussy, Y. Ni, Y. Zhou, J. Ye, and E. A. Cornell, "Precision measurement of the electron's electric dipole moment using trapped molecular ions," Phys. Rev. Lett. **119**, 153001 (2017).
[4] V. Andreev and N. Hutzler, "Improved limit on the electric dipole moment of the electron," Nature **562**, 355–360 (2018).
[5] C. Zhang, X. Zheng, and L. Cheng, "Calculations of time-reversal symmetry-violation sensitivity parameters based on analytic relativistic coupled-cluster gradient theory," Phys. Rev. A **104**, 012814 (2021).
[6] N. E. Shafer-Ray, "Possibility of 0-*g*-factor paramagnetic molecules for measurement of the electron's electric dipole moment," Phys. Rev. A **73**, 034102 (2006).
[7] M. G. Kozlov and L. N. Labzowsky, "Parity violation effects in diatomics," J. Phys. B: At., Mol. Opt. Phys. **28**, 1933 (1995).
[8] M. G. Kozlov, L. N. Labzowsky, and A. O. Mitrushenkov, "Parity nonconservation in diatomic molecules in strong constant magnetic field," J. Exp. Theor. Phys. **73**, 415 (1991); available at http://jetp.ras.ru/cgi-bin/e/index/e/73/3/p415?a=list.
[9] G. D. Rochester, "The band spectra of the lead halides, PbF and PbCI," Proc. R. Soc. London, Ser. A **153**, 407–421 (1936).
[10] F. Morgan, "Absorption spectra of PbF, PbCl and PbBr," Phys. Rev. **49**, 47 (1936).
[11] G. D. Rochester, "The band spectrum of lead fluoride (PbF). II," Proc. R. Soc. London, Ser. A **167**, 567–580 (1938).
[12] R. F. Barrow, D. Butler, J. W. C. Johns, and J. L. Powell, "Some observations on the spectra of the diatomic fluorides of silicon, germanium, tin, and lead," Proc. Phys. Soc., London, Sect. A **73**, 317 (1959).
[13] J. Chen and P. J. Dagdigian, "Laser fluorescence study of the Pb+F_2, Cl_2 reactions: Internal state distribution of the PbCl product and radiative lifetimes of PbF(A, B) and PbCl(A)," J. Chem. Phys. **96**, 1030–1035 (1992).
[14] R. B. Green, L. Hanko, and S. J. Davis, "Laser induced fluorescence studies of the $A^2\Sigma$ state of PbF," Chem. Phys. Lett. **64**, 461–464 (1979).
[15] O. Shestakov, A. M. Pravilov, H. Demes, and E. H. Fink, "Radiative lifetime and quenching of the $A^2\Sigma^+$ and $X_2{}^2\Pi_{3/2}$ states of PbF," Chem. Phys. **165**, 415–427 (1992).
[16] C. McRaven, P. Sivakumar, and N. Shafer-Ray, "Multiphoton ionization of lead monofluoride resonantly enhanced by the $X_1{}^2\Pi_{1/2} \rightarrow B^2\Sigma_{1/2}$ transition," Phys. Rev. A **75**, 024502 (2007).
[17] C. McRaven, P. Sivakumar, and N. Shafer-Ray, "Experimental determination of the hyperfine constants of the X_1 and A states of $^{207}Pb^{19}F$," Phys. Rev. A **78**, 054502 (2008).
[18] P. Sivakumar, C. McRaven, D. Combs, N. Shafer-Ray, and V. Ezhov, "State-selective detection of the PbF molecule by doubly resonant multiphoton ionization," Phys. Rev. A **77**, 062508 (2008).
[19] D. J. W. Lumley and R. F. Barrow, "Rotational analysis of the B-X_2, B-X_1 and A-X_1 systems of gaseous PbF," J. Phys. B: At. Mol. Phys. **10**, 1537 (1977).
[20] K. Ziebarth, K. D. Setzer, O. Shestakov, and E. H. Fink, "High-resolution study of the $X_2{}^2\Pi_{3/2} \rightarrow X_1{}^2\Pi_{1/2}$ fine structure transitions of PbF and PbCl," J. Mol. Spectrosc. **191**, 108–116 (1998).
[21] C. P. McRaven, P. Sivakumar, N. E. Shafer-Ray, G. E. Hall, and T. J. Sears, "Spectroscopic constants of the known electronic states of lead monofluoride," J. Mol. Spectrosc. **262**, 89–92 (2010).

[22]R. J. Mawhorter, B. S. Murphy, A. L. Baum, T. J. Sears, T. Yang, P. Rupasinghe, C. McRaven, N. Shafer-Ray, L. D. Alphei, and J.-U. Grabow, "Characterization of the ground X1 state of $^{204}Pb^{19}F$, $^{206}Pb^{19}F$, $^{207}Pb^{19}F$, and $^{208}Pb^{19}F$," Phys. Rev. A **84**, 022508 (2011).
[23]K. Balasubramanian, "Relativistic configuration interaction calculations of low-lying states of PbF," J. Chem. Phys. **83**(5), 2311–2315 (1985).
[24]H. Lefebvre-Brion and R. W. Field, *The Spectra and Dynamics of Diatomic Molecules* (Elsevier, 2004).
[25]S. Yamamoto and H. Tatewaki, "Excited states of PbF: A four-component relativistic study," J. Chem. Phys. **132**(5), 054303 (2010).
[26]H. Wang, A. T. Le, T. C. Steimle, E. A. C. Koskelo, G. Aufderheide, R. Mawhorter, and J.-U. Grabow, "Fine and hyperfine interaction in ^{173}YbF," Phys. Rev. A **100**, 022516 (2019).
[27]T. C. Steimle, T. Ma, and C. Linton, "The hyperfine interaction in the $A^2\mathbf{\Pi}_{1/2}$ and $X^2\mathbf{\Sigma}^+$ states of ytterbium monofluoride," J. Chem. Phys. **137**, 109901 (2012).
[28]J. M. Brown and A. Carrington, *Rotational Spectroscopy of Diatomic Molecules* (Cambridge University Press, Cambridge, 2003).
[29]C. M. Western, "PGOPHER: A program for simulating rotational, vibrational and electronic spectra," J. Quant. Spectrosc. Radiat. Transfer **186**, 221–242 (2017).
[30]L. Skripnikov, A. Kudashov, A. Petrov, and A. Titov, "Search for parity- and time-and-parity–violation effects in lead monofluoride (PbF): *Ab initio* molecular study," Phys. Rev. A **90**, 064501 (2014).
[31]K. Baklanov, A. Petrov, A. Titov, and M. Kozlov, "Progress toward the electron electric-dipole-moment search: Theoretical study of the PbF molecule," Phys. Rev. A **82**, 060501 (2010).
[32]M. G. Kozlov, V. I. Fomichev, Y. Y. Dmitriev, L. N. Labzovsky, and A. V. Titov, "Calculation of the P- and T-odd spin-rotational Hamiltonian of the PbF molecule," J. Phys. B: At. Mol. Phys. **20**, 4939 (1987).
[33]Y. Y. Dmitriev, Y. G. Khait, M. G. Kozlov, L. N. Labzovsky, A. O. Mitrushenkov, A. V. Shtoff, and A. V. Titov, "Calculation of the spin-rotational Hamiltonian including *P*- and *P*, *T*-odd weak interaction terms for HgF and PbF molecules," Phys. Lett. A **167**, 280–286 (1992).